Journal Pre-proof

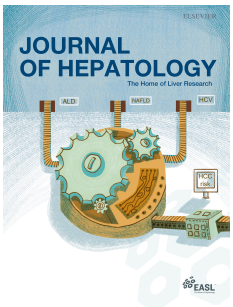

Single-nucleus profiling reveals hepatocyte identity and immune features associated with corticosteroid response in severe alcohol-related hepatitis

Lukas Van Melkebeke, Markus Boesch, Tessa Ostyn, Wenxin Huang, Cansu Akkaya, Matthias van Sligtenhorst, Dania El Abyad, Fateme Safaeifard, Alexander Dumarey, Marie Wallays, Bram Boeckx, Rita Feio-Azevedo, Lena Smets, Thierry Gustot, Eric Trepo, Christophe Moreno, Antonella Putignano, Luc Lasser, Isabelle Colle, Pierre Deltenre, Astrid Marot, Baki Topal, Eveline Claus, Lawrence Bonne, Geert Maleux, Colinda Scheele, Tim Hendrikx, Frederik Nevens, Hannelie Korf, Tania Roskams, Alexandre Denadai-Souza, Diether Lambrechts, Olivier Govaere, Schalk Van der Merwe, Jef Verbeek

PII: S0168-8278(26)00205-9

DOI: https://doi.org/10.1016/j.jhep.2026.04.002

Reference: JHEPAT 10500

To appear in: *Journal of Hepatology*

Received Date: 17 March 2025

Revised Date: 25 March 2026

Accepted Date: 11 April 2026

Please cite this article as: Van Melkebeke L, Boesch M, Ostyn T, Huang W, Akkaya C, van Sligtenhorst M, El Abyad D, Safaeifard F, Dumarey A, Wallays M, Boeckx B, Feio-Azevedo R, Smets L, Gustot T, Trepo E, Moreno C, Putignano A, Lasser L, Colle I, Deltenre P, Marot A, Topal B, Claus E, Bonne L, Maleux G, Scheele C, Hendrikx T, Nevens F, Korf H, Roskams T, Denadai-Souza A, Lambrechts D, Govaere O, Van der Merwe S, Verbeek J, Single-nucleus profiling reveals hepatocyte identity and immune features associated with corticosteroid response in severe alcohol-related hepatitis, *Journal of Hepatology*, https://doi.org/10.1016/j.jhep.2026.04.002.

Single-nucleus profiling reveals hepatocyte identity and immune features associated with corticosteroid response in severe alcohol-related hepatitis

Lukas Van Melkebeke[1,2,$], Markus Boesch[1,3,4,*], Tessa Ostyn[5,*], Wenxin Huang[1], Cansu Akkaya[6], Matthias van Sligtenhorst[6], Dania El Abyad[3,5], Fateme Safaeifard[7,8], Alexander Dumarey[1], Marie Wallays[1], Bram Boeckx[9,10], Rita Feio-Azevedo[1], Lena Smets[1,7,8], Thierry Gustot[11,12], Eric Trepo[11,12], Christophe Moreno[11,12], Antonella Putignano[11,13], Luc Lasser[13], Isabelle Colle[14], Pierre Deltenre[15,16,17], Astrid Marot[17], Baki Topal[18], Eveline Claus[19], Lawrence Bonne[19], Geert Maleux[19], Colinda Scheele[7,8], Tim Hendrikx[20], Frederik Nevens[1,2], Hannelie Korf[1], Tania Roskams[5], Alexandre Denadai-Souza[3,6], Diether Lambrechts[9,10], Olivier Govaere[3,5], Schalk Van der Merwe[1,2,**,$], Jef Verbeek[1,2,**,$]

[1]Laboratory of Liver Immunology, Hepatology Research Unit, Department of Chronic Diseased and Metabolism (CHROMETA), KU Leuven, Leuven, Belgium

[2]Department of Gastroenterology and Hepatology, University Hospitals Leuven, Leuven, Belgium

[3]KU Leuven Institute for Single Cell Omics, KU Leuven, Leuven, Belgium

[4]Laboratory of Reproductive Genomics, Department of Human Genetics, KU Leuven, Leuven, Belgium

[5]Department of Imaging and Pathology, Translational Cell and Tissue Research, KU Leuven and University Hospitals Leuven, Leuven, Belgium

[6]Laboratory of Mucosal Biology, Hepatology Research Unit, Department of Chronic Diseased and Metabolism (CHROMETA), KU Leuven, Leuven, Belgium

[7]Laboratory for Intravital Imaging and Dynamics of Tumor Progression, VIB Center for Cancer Biology, Leuven, Belgium.

[8]Department of Oncology, KU Leuven, Leuven, Belgium

[9]Laboratory for Translational Genetics, Department of Human Genetics, KU Leuven, Leuven, Belgium

[10]VIB Center for Cancer Biology, Leuven, Belgium

[11]Department of Gastroenterology, Hepatopancreatology and Digestive Oncology, Hôpital Universitaire de Bruxelles, Université Libre de Bruxelles, Brussels, Belgium

[12]Laboratory of Experimental Gastroenterology, Université Libre de Bruxelles, Brussels, Belgium.

[13]Department of Hepatogastroenterology, Centre Hospitalier Universitaire Brugmann, Brussels, Belgium

[14]Department of Gastroenterology and Hepatology, A-Zorg campus Merestraat, Aalst, Belgium

[15]Department of Gastroenterology and Hepatology, Clinique St-Luc, Bouge, Belgium

[16]Department of Gastroenterology, Hepatology and Digestive Oncology, CUB Hôpital Erasme, Université Libre de Bruxelles, Brussels, Belgium

[17]Department of Gastroenterology and Hepatology, CHU UCL Namur, Université Catholique de Louvain, Yvoir, Belgium

[18]Department of Abdominal Surgery, University Hospitals Leuven, Leuven, Belgium

[19]Department of Interventional Radiology, UZ Leuven, Leuven, Belgium

[20]Department of Laboratory Medicine, Medical University of Vienna, Vienna, Austria

* Shared contribution

** Shared contribution

$ Corresponding Author:

Corresponding author

Dr. Lukas Van Melkebeke
Hepatology research unit,
Department of Chronic Diseases, Metabolism and Ageing (CHROMETA),
KU Leuven, Herestraat 49, Leuven 3000, Belgium
lukas.vanmelkebeke@kuleuven.be

Prof. dr. Schalk van der Merwe
Hepatology research unit,
Department of Chronic Diseases, Metabolism and Ageing (CHROMETA),
KU Leuven, Herestraat 49, Leuven 3000, Belgium
schalk.vandermerwe@uzleuven.be

Prof. dr. Jef Verbeek
Hepatology research unit,
Department of Chronic Diseases, Metabolism and Ageing (CHROMETA),
KU Leuven, Herestraat 49, Leuven 3000, Belgium
jef.verbeek@uzleuven.be

Short title

Sn-RNAseq of sAH defines treatment response

Conflicts of interest

No conflicts of interest declared.

Author Contributions

LVM: Sample collection, Data analysis, Validation, Writing – original draft, Writing – review and editing, Funding, Conceptualization; **MB**: Data analysis, Writing – review and editing; **TO**: Data analysis, Validation, Writing – review and editing; **WH**: Sample collection, Data analysis, Writing – original draft, Validation, Writing – review and editing; **CA**: Data analysis,

Validation, Writing – original draft, Writing – review and editing; **MVS**: Data analysis, Validation, Writing – review and editing; **DEA**: Data analysis, Writing – review and editing; **FS**: Data analysis, Writing – review and editing; **AD**: Data analysis, Writing – review and editing; **MW**: Sample collection, Data analysis, Writing – review and editing; **BB**: Data analysis, Writing – review and editing; **RFA**: Sample collection, Writing – review and editing; **LS**: Sample collection, Writing – review and editing; **TG**: Sample collection, Writing – review and editing; **ET**: Sample collection, Writing – review and editing; **CM**: Sample collection, Writing – review and editing; **AP**: Sample collection, Validation, Writing – review and editing; **LL**: Sample collection, Validation, Writing – review and editing; **IC**: Sample collection, Writing – review and editing; **PD**: Sample collection, Validation, Writing – review and editing; **AM**: Sample collection, Validation, Writing – review and editing; **BT**: Sample collection, Writing – review and editing; **EC**: Sample collection, Writing – review and editing; **LB**: Sample collection, Writing – review and editing; **GM**: Sample collection, Writing – review and editing; **CS**: Data analysis, Writing – review and editing; **TH**: Validation, Writing – review and editing; **FN**: Sample collection, Writing – review and editing; **HK**: Data analysis, Writing – original draft, Writing – review and editing, Funding; **TR**: Data analysis, Validation, Writing – review and editing, Funding; **ADS**: Data analysis, Validation, Writing – review and editing; **DL**: Data analysis, Writing – review and editing, Funding; **OG**: Data analysis, Validation, Writing – original draft, Writing – review and editing, Funding, Conceptualization; **SVDM**: Sample collection, Validation, Writing – original draft, Writing – review and editing, Funding, Conceptualization; **JV**: Sample collection, Validation, Writing – original draft, Writing – review and editing, Funding, Conceptualization

Funding

This study was supported by a research grant from The Research Foundation – Flanders (FWO; Fonds voor Wetenschappelijk Onderzoek – Vlaanderen) (G082018N to SVDM, G032324N to OG), LVM (1110121N) received a junior research mandate and SVDM a senior research mandate from FWO. Additionally, our research was supported by internal funding from KU Leuven (C14/18/087, C14/23/135 & AKUL/19/039). Financial support was also received from the Belgian Association for the Study of the Liver and a research grant from the Belgian Week of Gastroenterology (BWGE) to LVM and an internal KU Leuven fund to JV.

Keywords

Severe alcohol-related hepatitis; alcohol-related liver disease; single-nucleus sequencing; hepatocyte biology; treatment response

Highlights

- A single-nucleus atlas of sAH liver samples captures baseline and early corticosteroid-associated cellular changes
- Corticosteroid responders show a higher baseline proportion of liver-infiltrating monocytes
- Loss of mature hepatocyte identity is a hallmark of sAH and is more pronounced in non-responders
- SULT2A1 staining predicts corticosteroid response at baseline, including in patients with infection and ACLF
- Therapeutic corticosteroid response is characterized by enhanced hepatocyte regeneration at day 8 of treatment

Abstract

Background & Aims: Severe alcohol-related hepatitis (sAH) is associated with high short-term mortality. However, 30–40% of patients fail to respond to corticosteroids, the only proven pharmacological treatment. The pathophysiological mechanisms underlying sAH and the marked heterogeneity in treatment response remain incompletely understood. We aimed to define cellular changes associated with corticosteroid response in sAH and to identify baseline markers predictive of treatment outcome.

Methods: Single-nucleus RNA sequencing was performed on liver biopsies from patients with biopsy-proven sAH (n=17), including paired baseline and day 8 biopsies in a subset (n=8). Patients were classified as corticosteroid responders (sAH-R; Lille score <0.45) or non-responders (sAH-NR; Lille score ≥0.45). Liver biopsies from patients with acute decompensation of alcohol-related liver disease (AD; n=5) and healthy controls (n=4) were included for comparison. Findings were validated using immunohistochemistry and spatial proteomics in a large multicenter validation cohort (n=172).

Results: At baseline, sAH-R patients exhibited a significantly higher proportion of liver-infiltrating S100A8+ monocytes compared to sAH-NR, a difference that persisted at day 8. sAH livers showed a marked reduction in mature hepatocytes and an expansion of stressed and intermediate hepatocyte populations compared to AD and healthy liver, indicating progressive loss of mature hepatocyte identity. This loss was more pronounced in sAH-NR patients, who also exhibited fewer cycling hepatocytes at day 8, consistent with impaired regenerative capacity. Expression of SULT2A1, a marker of mature hepatocyte identity, was significantly reduced in sAH-NR at baseline. Finally, liver biopsies with ≥50% SULT2A1-positive hepatocytes at baseline were strongly predictive of corticosteroid response.

Conclusions: This study delineates distinct immune and hepatocyte changes associated with corticosteroid response in sAH. Baseline SULT2A1 expression may facilitate stratified treatment approaches in sAH.

Impact and implications

Severe alcohol-related hepatitis (sAH) represents one of the most devastating manifestations of alcohol-related disorders. sAH is characterized by acute hepatic inflammation and high short-term mortality. Clinical management remains challenging, as corticosteroids - the only pharmacological therapy currently applied - are ineffective in a substantial proportion of patients and are associated with significant adverse effects. These limitations highlight the need for a more detailed understanding of sAH pathophysiology and for approaches that enable improved patient stratification and therapeutic decision-making.

In this study, we identify distinct pre-treatment differences between corticosteroid responders and non-responders at the level of both hepatocytes and myeloid cells, providing new insight into the cellular mechanisms underlying treatment heterogeneity in sAH. Furthermore, leveraging these findings, we developed a histology-based SULT2A1 scoring system using a commercially available antibody, which predicts corticosteroid response at baseline and may support stratified treatment approaches in clinical practice.

Introduction

Alcohol-related liver disease (ALD) is a leading cause for liver disease and cirrhosis-related deaths globally[1]. ALD typically progresses slowly, evolving from steatosis to fibrosis and eventually cirrhosis[1]. Some patients develop alcohol-related hepatitis (AH), an acute manifestation of ALD that usually occurs in the context of pre-existing cirrhosis[1,2]. AH varies in severity, and severe alcohol-related hepatitis (sAH) represents a distinct clinical syndrome characterized by recent-onset jaundice and systemic inflammation in patients with chronic alcohol use disorder[1,2]. sAH is defined by a Maddrey discriminant function (MDF) ≥32 and/or a Model for End-Stage Liver Disease (MELD) score ≥20[1,2]. Patients presenting with sAH face significant short- and long-term mortality, with rates reaching 30% at 3 months and 45% at one year[1,3].

Despite its high mortality, therapeutic options for sAH remain limited[1,4]. Corticosteroids are the only pharmacological treatment currently used in clinical practice, offering improved survival at one month[5]. However, around 30-40% of patients with sAH fail to respond to corticosteroid therapy, as determined by the Lille-score on day 7 of treatment[2,3,6]. For these non-responders, corticosteroid therapy is discontinued, resulting in a dismal prognosis, with mortality reaching 60% at six months[3,6]. Moreover, corticosteroid use has been associated with an increased risk of infections, which are linked to even higher mortality rates in sAH patients[7]. Future research aimed at identifying novel therapeutic targets and improving prognostic prediction prior to corticosteroid treatment is critical in the management of sAH.

The absence of baseline predictors and the lack of effective novel therapies likely reflect an incomplete understanding of sAH pathophysiology. Bulk transcriptomic studies have suggested that sAH is characterized by impaired hepatocyte regeneration and progressive hepatocyte loss-of-identity, resulting in loss of metabolic function and accumulation of immature hepatocytes[8–11]. In parallel, gene deconvolution approaches have identified expansion of pro-inflammatory myeloid cell populations in sAH compared to other chronic liver diseases[10]. More recently, single-cell and single-nucleus RNA sequencing (scRNA-seq and snRNA-seq) have revealed the cellular complexity of healthy and diseased livers, underscoring the limitations of bulk approaches[12,13]. However, it remains unclear whether disease-associated hepatocyte and myeloid cell changes influence corticosteroid responsiveness or could serve as predictive markers at baseline.

To address these gaps, we leveraged a two-tiered study design. First, we generated a baseline snRNA-seq atlas spanning healthy liver, acute decompensation ALD cirrhosis (AD), and a large cohort of patients with sAH to define disease-associated immune and hepatocyte changes. Second, we performed sequential snRNA-seq on paired liver biopsies obtained at baseline, before start of corticosteroid therapy, and at day 8 in a well-characterized subset of sAH patients, enabling interrogation of early temporal cellular changes following corticosteroid therapy.

We correlated the transcriptomic results with large multicenter histological validation cohorts and functional perturbation studies to define cellular changes underlying corticosteroid response in sAH. We identify two complementary biological axes associated with therapeutic response: a corticosteroid-responsive inflammatory myeloid state and preserved baseline mature hepatocyte identity marked by SULT2A1 expression. Together, these findings provide mechanistic insight into response heterogeneity and establish a clinically applicable framework for baseline patient stratification

Patients and methods

Patient population and sample collection

This study analyzed 34 liver tissue samples by snRNA-seq and 172 liver tissue samples in an multicentric validation cohort. The snRNA-seq cohort comprised liver biopsies from healthy controls (n = 4), AD patients (n = 5), and patients with sAH (n = 17). Among the sAH patients, 9 were corticosteroid responders (sAH-R; Lille score < 0.45) and 8 were non-responders (sAH-NR; Lille score ≥ 0.45). Sequential biopsies obtained at day 8 were available for 8 sAH patients (4 sAH-R and 4 sAH-NR). Biopsies were collected at University Hospitals Leuven (Belgium; S54588, S63593, S64744) and the Université Libre de Bruxelles (Belgium; B2015/515). Spatial proteomics (COMET) was performed on liver biopsies from patients with sAH (n = 2; 28,022 cells), collected at University Hospitals Leuven (Belgium; S64744).

The histological validation cohort comprised liver tissue from multiple clinical groups: healthy controls (n = 8), ALD explants (n = 10), AD patients (n = 11), and patients with sAH. The sAH cohort included patients treated with corticosteroids at baseline (n = 102; 72 sAH-R and 30 sAH-NR), patients who did not receive corticosteroids (n = 29; 17 responders and 12 non-responders), and patients with sAH treated with corticosteroids who underwent biopsy at day 8 (n = 12; 8 sAH-R and 4 sAH-NR).

Biopsies were collected at University Hospitals Leuven (Belgium; S67418, S63593), Centre Hospitalier Universitaire Brugmann (CHU) ((Belgium; CE 2025/94), CHU UCL Namur Site Godinne (Belgium; 229.2024), Clinique Saint-Luc (Belgium; CE-SLBO2024-09), and Université Libre de Bruxelles (Belgium; B2015/515).

Detailed inclusion and exclusion criteria are provided in the Supplementary Methods. Clinical characteristics of all patient groups are summarized in Tables S1–S4. Ethical approval was obtained from the appropriate institutional review boards at all participating centers, and written informed consent was obtained from all patients.

Single-nucleus RNA-sequencing & data-analysis

The detailed description and the script used can be found in the supplementary methods. In short, liver biopsies were mechanically homogenized after snap freezing. snRNA-seq was performed using the Chromium Single Cell 3’ Library Kit (v3.1, 10x Genomics) and the NovaSeq 6000 platform (Illumina). Raw sequencing reads were aligned to the human reference

genome (GRCh38/hg38) and demultiplexed using CellRanger (v3.0.2). Ambient RNA contamination was removed with SoupX (v.1.6.2). For downstream analysis, the resulting gene-cell matrix was processed in Seurat (v4.1.1, v5.3.0). After quality control and doublet identification via DoubletFinder (v2.0.3, v2.0.6), gene expression data was integrated using an anchor-based approach. Clusters representing liver cell populations were combined and labeled based on previously published canonical markers[12–15]. Subclustering was performed for further analysis. The miloR package (v2.4.1) was utilized for differential abundance testing. Pathway analysis was conducted using the GSVA package (v1.42.0) in R for single-sample gene set enrichment analysis. A pseudotime trajectory was constructed using monocle (v2.36.0). Cell-cell communication analysis was performed using the CellChat R package (v2.0.0). The single-nucleus atlas was developed using R shiny (v.1.11.1) and the ShinyCell R package (v.2.1.0).

Deconvolution

To validate hepatocyte and cholangiocyte population shifts observed in the single-nucleus dataset, we performed RNA-seq deconvolution of publicly available bulk liver transcriptomic datasets (GSE143318, GSE270042, and GSE167308) using CIBERSORTx)[9,25,26]. Cell-type signature matrices were derived from the snRNA-seq data and used to estimate relative cell-type abundances in bulk samples. This analysis enabled cross-cohort assessment of parenchymal cell-state changes associated with severe alcohol-related hepatitis. Detailed preprocessing, normalization, and signature generation procedures are described in the Supplementary Methods.

Immunohistochemistry

The full immunohistochemistry protocol is provided in the Supplementary Methods. Briefly, immunohistochemistry (IHC) was performed on formalin-fixed, paraffin-embedded liver sections using a fully automated BOND Max staining platform (Leica Microsystems). Whole-slide images were acquired using a Zeiss Axioscan.Z1 digital slide scanner.

For S100A8 and AKR1B10, quantitative image analysis was performed using ImageJ, calculating the area of positive staining relative to the total tissue area. In contrast, SULT2A1 and Ki67 staining were assessed by semi-quantitative histological scoring. All slides were evaluated in a blinded fashion by an expert liver pathologist (T.R.). SULT2A1 was scored based on the proportion of hepatocytes exhibiting positive staining relative to the total hepatocyte population, whereas Ki67 was quantified as the number of positive hepatocytes per high-power field.

For SULT2A1, we defined four grades of positivity:
Grade 3: >95% of hepatocytes positive.
Grade 2: 50–94% of hepatocytes positive.
Grade 1: 5–49% of hepatocytes positive.
Grade 0: <5% of hepatocytes positive.

Spatial proteomics

Sequential multiplex immunofluorescence was performed using the COMET® platform (Lunaphore Technologies) as described in the Supplementary Methods. High-resolution images were acquired and processed using the HORIZON® software suite (v2.3.0, Lunaphore Technologies). Cell segmentation was conducted separately for each region of interest using deep learning–based algorithms guided by phenotypic markers, including CD68, SULT2A1, TNFα, CD4, CD3, CD31, αSMA, MARCO, CK7, and CK18. Downstream quantitative analyses were performed in R(v4.5.0).

In vitro experiments

The full protocol is provided in the Supplementary Methods. Briefly, two single-guide RNAs (sgRNAs) targeting exon 2 of *SULT2A1* were designed using the SYNTHEGO gRNA design tool. For each electroporation, pooled sgRNAs (300 pmol total; IDT) were complexed with Cas9-HiFi nuclease (40 pmol; IDT). HepG2 cells were electroporated using the NEPA21 system. At 72 hours post-electroporation, GFP-positive cells were isolated by fluorescence-activated cell sorting (SONY MA900, KU Leuven FACS Core), seeded into 48-well plates, and subsequently expanded to 6-well plates. Upon reaching confluency, cells were harvested and used for downstream imaging and flow cytometry analyses.

General statistics

Continuous variables are presented as mean ± standard deviation for normally distributed data and as median with interquartile range for non-normally distributed data. Normality was assessed using the Shapiro–Wilk test. All statistical tests were two-sided, and a p-value < 0.05 was considered statistically significant. In cases of highly significant results, only the lowest p-values are reported. Multivariate analyses were performed using logistic regression models with corticosteroid response, defined by the Lille score, as the dependent variable. Statistical

analyses and graphical representations were generated using GraphPad Prism (v10.0; GraphPad Software) and R (v4.1.2) with the relevant packages.

Results

Development of a hepatic single-nucleus transcriptomic atlas across the ALD spectrum

To define cellular changes across the spectrum of ALD and to investigate mechanisms underlying corticosteroid response in sAH, we generated a snRNA-seq atlas of human liver biopsies. In total, 34 liver biopsies were analysed, including samples from healthy controls (n = 4), AD patients (n = 5), and patients with biopsy-proven sAH (n = 17). Among sAH patients, 9 were classified as sAH-R and 8 as sAH-NR based on the Lille score at day 7. Within this sAH cohort, paired baseline, before start of corticosteroid therapy, and day 8 biopsies were available for a subset of 8 patients (4 sAH-R and 4 sAH-NR) (Fig.1A, Tables S1, S5). Following data processing and integration, the final dataset, including baseline and paired samples, comprised 381,812 high-quality nuclei. Unsupervised clustering identified eight major hepatic cell types, which were further resolved into 38 transcriptionally distinct cell types (Fig.1B–C, Fig.S1A-E)[12,13,15,16]. An interactive Shiny application was developed to enable public exploration of the sAH single-nucleus transcriptomic atlas (http://ccb-bioit.shinyapps.io/sn-ah-atlasbrowser.

Across disease stages, comparison of major cell-type proportions revealed significant differences between healthy and cirrhotic livers (AD and sAH), including a decreased proportion of hepatocytes and increased proportions of cholangiocytes and mesenchymal cells in cirrhotic livers, consistent with prior observations (Fig.1D)[13,14]. No significant differences regarding proportions in major cell-type composition were observed between sAH-R and sAH-NR. Subsequent analyses therefore focused on myeloid cells and hepatocytes, in which the most pronounced disease- and response-associated transcriptional differences were observed.

Single nucleus sequencing of sequential liver biopsies reveals an influx of monocytes in sAH corticosteroid-responders.

To determine whether immune cell composition differs between corticosteroid responders and non-responders before start of treatment, we first examined the myeloid compartment in the snRNA-seq dataset. While no differences were observed in the proportion of major hepatic cell types, significant differences emerged within the myeloid population when comparing sAH-R and sAH-NR (Fig.2A–D).

Subclustering of myeloid cells identified seven transcriptionally distinct populations: two mature macrophage clusters: Kupffer cells and GPNMB^{high} macrophages, an intermediate cluster that we annotated STAB1/F13A1^{high} macrophages, monocytes, cDC1, cDC2, and cycling myeloid cells (Fig.2A–B, Fig.S2A–B; Supplementary Results). Differential abundance analysis using MiloR revealed a significantly higher proportion of monocytes in sAH-R compared to sAH-NR patients, both at baseline and at day 8 (Fig.2C–D).

Following corticosteroid therapy, monocytes from both sAH-R and sAH-NR, exhibited transcriptional changes consistent with glucocorticoid exposure, including upregulation of corticosteroid-responsive genes such as *ADAMTS2* and *FKBP5* and downregulation of inflammatory pathways at day 8 (Fig.2E, Fig.S2C)[17]. In parallel, cell–cell communication analysis demonstrated a reduction in interactions between monocytes and other hepatic cell types following treatment (Fig.S2D).

To validate these findings, we performed immunohistochemistry for S100A8—a pro-inflammatory marker selectively enriched in monocytes in the snRNA-seq dataset—in a large multicenter cohort of human liver biopsies (n = 93). In addition, spatial proteomics (COMET) was performed in a subset of samples (n = 2) to provide spatially resolved confirmation of monocyte-associated S100A8 expression (Fig.1C)[18,19]. At baseline, the S100A8-positive area was significantly greater in corticosteroid responders compared with non-responders (Fig.2F–H, Fig.S2E). In contrast, no difference in S100A8 staining was observed in a separate cohort of sAH patients who did not receive corticosteroid therapy, irrespective of clinical outcome (Fig.S2F).

Together, these data indicate that corticosteroid responders are characterized by baseline monocyte infiltration that is responsive to steroid-mediated immunomodulation. We next investigated whether, alongside this immune axis, baseline hepatocyte identity and functional maturity also differ between responders and non-responders and could contribute to divergent clinical recovery.

Severe alcohol-related hepatitis is characterized by progressive loss of mature hepatocyte identity, with a further deterioration in non-responders.

Consistent with previously described zonation-associated transcriptional signatures, hepatocyte subclustering identified five distinct populations (Fig.3A,B, Fig.S3A)[20]. Central venous hepatocytes (e.g. *CYP2E1*, *SLCO1B3*) and periportal hepatocytes (e.g. *HAL*, *SDS)* predominated in healthy liver samples (Fig.3C)[20]. In contrast, cirrhotic livers, were enriched for two additional hepatocyte populations. Stressed hepatocytes were characterized by reduced expression of mature hepatocyte markers (e.g. *HNF4α*, *SULT2A1*, *ASGR1*) and increased expression of genes associated with endoplasmic reticulum stress, ballooned hepatocytes, and apoptosis (e.g. *AKR1B10*, *DAPK2*, *SQSTM1*) (Fig.3A,B,D)[21,22]. Pathway analysis confirmed enrichment of apoptosis, autophagy, cytokine production, oxidative stress, and endoplasmic reticulum stress pathways in this population (Fig.S3A). A second population increased in cirrhotic livers, termed intermediate hepatocytes, exhibited a further loss of mature hepatocyte identity with concurrent expression of cholangiocyte-associated markers (e.g. *KRT7*, *CFTR*) (Fig.3A,B,D, Fig.S3B)[9,23,24]. The presence of intermediate $K7^+$ hepatocytes was independently confirmed by spatial proteomics (COMET) (Fig.S3C). Pseudotime analysis positioned intermediate hepatocytes between stressed hepatocytes and cholangiocytes, consistent with a transitional type (Fig.3E). Finally, a small population of cycling hepatocytes was identified based on high expression of cell cycle–related genes (Fig.3A–B).

Across disease stages, there was a marked frequency shift from mature central venous and periportal hepatocytes toward stressed and intermediate populations in AD and sAH compared to healthy liver (Fig.3C). This shift was more pronounced in sAH than in AD, with a significantly higher proportion of intermediate hepatocytes and a trend toward fewer central venous hepatocytes in sAH ($p_{adj} = 0.053$) (Fig.3C). Deconvolution of independent bulk RNA-seq datasets validated this progressive loss of mature hepatocytes in sAH relative to AD and healthy liver (Fig.S3D–E)[9,25]. Notably, partial reversal of this shift was observed in sAH patients surviving to day 28, suggesting potential recovery of mature hepatocyte identity in favorable outcomes (Fig.S3F)[26].

At treatment baseline, hepatocytes from sAH-NR exhibited, transcriptionally, a more pronounced loss of mature hepatocyte identity compared to sAH-R (Fig.3F,G, Fig.S4A). sAH-NR hepatocytes showed downregulation of key periportal and central venous hepatocyte genes (*ALB*, *CYP2C9*, *PCK1*, *SLCO1B3*, *BHMT*), alongside reduced expression of critical mature hepatocyte markers (*HNF4α*, *ASGR1*) (Fig.3G, Fig.S4A)[9]. Conversely, genes characteristic of

less mature hepatocyte populations, including *CTNNA2* and *FGF13*, were upregulated in hepatocytes from sAH-NR. (Fig.3B,G, Fig.S4A).

These transcriptomic findings were validated by immunohistochemistry in a large multicenter cohort (n = 131). Expression of AKR1B10, a marker of stressed and intermediate hepatocytes, was significantly increased in explant and sAH samples compared to healthy liver and was higher in sAH than in explant samples (Fig.4A–C). In contrast, SULT2A1, a marker upregulated in central venous and periportal hepatocytes, was significantly reduced in explant, AD, and sAH samples compared to healthy liver, with a further decrease in sAH compared to explants and a trend toward lower expression in sAH compared to AD ($p = 0.07$) (Fig.4D-E, Fig.S4A-B). Importantly, SULT2A1 staining was significantly lower in sAH-NR compared to sAH-R (Fig.4E–G).

SULT2A1 expression in transjugular liver biopsies predicts corticosteroid response at baseline

Given the pronounced loss of gene signatures defining mature hepatocytes in sAH-NR, we next sought to identify a clinically applicable marker indicating preservation of hepatocyte maturity at baseline. Among genes consistently downregulated in sAH-NR compared to sAH-R hepatocytes, *SULT2A1* emerged as a top candidate, both across all hepatocytes and within central venous, periportal, and stressed hepatocyte subpopulations (Fig.3G, Fig.S5A–B). SULT2A1 expression was highly hepatocyte-specific (Fig.1C) and expressed in both mature central venous and periportal hepatocytes, with immunohistochemical staining observed in >95% of hepatocytes in healthy liver samples (Fig.S4B). Importantly, mean transcriptomic *SULT2A1* expression correlated strongly with histological SULT2A1 grading in paired samples ($r = 0.69$, $p < 0.001$), supporting the use of IHC-based scoring as a surrogate for transcriptional *SULT2A1* expression. (Fig.5A).

Comparative analysis of *SULT2A1*-positive and -negative hepatocytes revealed that *SULT2A1*-positive cells were enriched for markers of mature periportal and central venous hepatocytes and for genes critical to hepatocyte maturation and function (e.g. *SLCO1B3, HAL, ALB, HNF4a, ASGR1*) (Fig.5B). In contrast, *SULT2A1*-negative hepatocytes showed increased expression of genes characteristic of stressed and intermediate hepatocytes and cholangiocyte markers (e.g. *FGF13, CFTR, KRT7*) (Fig.5B). Consistently, pathway analysis demonstrated

enrichment of mature hepatocyte metabolic and detoxification pathways in *SULT2A1*-positive hepatocytes across all hepatocyte subtypes, whereas these pathways were markedly reduced in *SULT2A1*-negative cells (Fig.5C, Fig.S5C–F). These findings position *SULT2A1* as an integrative marker of mature hepatocyte identity. Based on these features, we investigated whether SULT2A1 expression at baseline could predict corticosteroid response.

In transjugular liver biopsies, samples with ≥50% SULT2A1-positive hepatocytes at baseline (grades 2–3) were nearly four times more likely to be derived from corticosteroid responders compared to samples with grades 0–1 (59.7% vs. 16.7%, $p < 0.0001$), yielding a positive predictive value of 89.6% (Fig.5D). Importantly, this association remained significant in clinically challenging subgroups, including patients with active infection at baseline (n=29) and those with acute-on-chronic liver failure (ACLF) grade 2–3 (n=18) (Fig.5E).

SULT2A1 grade was significantly associated with 30-day mortality ($p < 0.05$) but not with longer-term survival (Fig.5F). In a cohort of sAH patients who did not receive corticosteroid therapy (n = 29) there was no difference in SULT2A1 score between patients with favorable and unfavorable clinical outcomes, but a small significant difference in SULT2A1 expression (grade) was present (Fig.5G), suggesting partial specificity for treatment responsiveness.

At baseline, SULT2A1 grade was negatively correlated with serum bilirubin levels and parenchymal bilirubinostasis and showed a trend toward positive correlation with albumin levels ($r = 0.20$, $p = 0.07$) (Fig.5H), supporting its association with preserved mature hepatocyte function. SULT2A1 grade also correlated positively with S100A8 staining, linking mature hepatocyte identity to the inflammatory myeloid axis identified earlier (Fig.5H). In contrast, no correlation was observed with commonly used prognostic scores, including MELD, MDF, and Child–Pugh (Fig.5H). Longitudinally, baseline SULT2A1 grade correlated with Lille score ($r = -0.34$, $p < 0.001$), absolute bilirubin reduction ($r = -0.21$, $p < 0.05$), and the percentage of bilirubin reduction ($r = -0.28$, $p < 0.01$). In multivariate logistic regression analyses, SULT2A1 grade remained independently associated with Lille response even after adjustment for MDF and MELD scores, as well as after adjustment for baseline Lille score parameters (age, bilirubin, creatinine, INR), indicating that SULT2A1 provides predictive information beyond existing clinical metrics (Table S6).

Corticosteroid responders exhibit enhanced hepatocyte regenerative activity at day 8

To determine whether preserved mature hepatocyte identity translates into differential regenerative responses following therapy, we examined hepatocyte transcriptional changes and proliferative activity in sequential liver biopsies.

By day 8 of corticosteroid treatment, both sAH-R and sAH-NR exhibited partial restoration of hepatocyte metabolic pathways, including nitrogen compound detoxification and fatty acid oxidation, alongside a reduction in pathways associated with cellular senescence, consistent with partial recovery of hepatocyte function (Fig.6A). In contrast, hepatocytes from sAH-NR patients retained significant upregulation of senescence-associated pathways at day 8 (Fig.6A). Moreover, hepatocyte growth factor receptor signaling—a key pathway involved in liver regeneration—was consistently more active in sAH-R patients at both baseline and day 8 (Fig.6A), suggesting sustained regenerative signaling in responders. Moreover, sAH-R patients demonstrated a significantly higher proportion of cycling hepatocytes at day 8 compared to sAH-NR patients (Fig.6B). Importantly, differences in proliferative capacity were already evident at baseline. Hepatocytes from sAH-R patients displayed higher expression of cell cycle–related genes prior to therapy, a pattern that was also observed in *SULT2A1*-positive hepatocytes irrespective of response status (Fig.5B, Fig.6C). Consistently, pathways related to hepatocyte proliferation and regeneration were enriched in *SULT2A1*-positive compared to *SULT2A1*-negative hepatocytes (Fig.5C).

To validate these findings at the tissue level, we performed immunohistochemistry on liver biopsies obtained at day 8 from sAH patients (n = 14). Expression of Ki67, a marker of cellular proliferation, was significantly higher in sAH-R compared to sAH-NR patients (Fig. 6D–E), confirming increased hepatocyte proliferative activity in responders

To explore whether SULT2A1 expression is functionally linked to hepatocyte proliferative capacity, we generated a *SULT2A1* knockout (KO) HepG2 cell line using CRISPR–Cas9 genome editing (Fig.S6A-D). Flow cytometry-based assessment of CellTrace Violet signal intensity loss after proliferation indicated that SULT2A1-deficient cells exhibited a significantly reduced growth rate compared to control cells, accompanied by markedly lower Ki67 expression (Fig.S6B,D–I).

Together, these data support a model in which preserved mature hepatocyte identity, reflected by SULT2A1 expression, is associated with enhanced regenerative competence, providing biological plausibility for the link between baseline hepatocyte differences and therapeutic response in sAH.

Discussion

sAH remains a life-threatening condition with limited therapeutic options and marked heterogeneity in response to corticosteroid therapy. Although corticosteroids provide a modest short-term survival benefit, up to 40% of patients fail to respond, and no validated baseline biomarkers currently exist to guide treatment initiation[27]. In this study, we combined single-nucleus transcriptomics, computational deconvolution of independent bulk liver transcriptomic datasets, spatial proteomics, extensive histological validation, and functional validation experiments to delineate the cellular changes underlying corticosteroid response in sAH and to identify clinically actionable baseline predictors.

By generating a snRNA-seq atlas comprising more than 380,000 nuclei across healthy liver, AD, and sAH—including sequential biopsies—we uncovered two complementary biological axes that together shape therapeutic response.

The first axis is immunological. At baseline, corticosteroid responders exhibited an enrichment of pro-inflammatory monocytes, a population that showed marked transcriptional suppression and reduced ligand–receptor–mediated cell–cell communication following corticosteroid therapy. This finding suggests that responders enter treatment with an inflammatory state that is amenable to steroid-mediated immunomodulation. Notably, this baseline enrichment of pro-inflammatory monocytes was not observed in untreated patients when stratified by clinical outcome, supporting the interpretation that this myeloid state is specifically associated with corticosteroid responsiveness rather than general disease severity. While it is plausible that heightened inflammation renders these patients more susceptible to anti-inflammatory therapy, pro-inflammatory cytokines such as IL-6 and TNF are also known to support liver regeneration, raising the possibility that monocytes may simultaneously facilitate tissue repair[28].

The second axis is parenchymal and centers on mature hepatocyte identity and regenerative competence. Across the ALD spectrum, we observed a progressive shift from mature periportal and central venous hepatocytes toward stressed and intermediate hepatocytes, reflecting attenuation of gene signatures characteristic of mature hepatocytes[11]. This shift was most pronounced in sAH and further accentuated in corticosteroid non-responders. Among markers associated with hepatocyte maturity, SULT2A1 emerged as a robust and hepatocyte-specific marker linked to preserved mature hepatocytes, metabolic function, and regenerative signaling.

At the molecular level, SULT2A1 expression correlated strongly with transcriptional features of mature hepatocytes and with preserved metabolic and detoxification pathways. *SULT2A1* encodes a cytosolic sulfotransferase that catalyzes the sulfonation of bile acids, steroid hormones, and xenobiotics, thereby contributing to hepatic metabolic homeostasis and protection from toxic intermediates[29]. At the tissue level, higher SULT2A1 positivity co-occurred with increased S100A8-positive monocyte infiltration, a myeloid profile characteristic of corticosteroid responders.

SULT2A1-positive hepatocytes were enriched for transcriptional signals related to steroid hormone responsiveness and regenerative signaling, including growth factor receptor–mediated proliferative pathways, consistent with preserved hepatocyte functional competence. This observation aligns with recent proteomic data demonstrating altered glucocorticoid receptor expression and disrupted steroid metabolism in corticosteroid non-responders[30]. Beyond its established role in bile acid and steroid metabolism, reduced *SULT2A1* expression has been associated with attenuation of mature hepatocyte transcriptional programs and adverse prognosis in hepatocellular carcinoma, further supporting its relevance as a marker of hepatocyte functional reserve[29,31]. Finally, while SULT2A1 expression also associates with clinical outcome in untreated patients, its strongest predictive value emerges in the context of corticosteroid therapy, indicating that it captures baseline disease biology that modulates therapeutic responsiveness rather than treatment-independent survival alone.

Building on these biological associations, we developed a semi-quantitative, histology-based SULT2A1 scoring system to assess baseline hepatocyte functional reserve in sAH. This score predicted corticosteroid response prior to treatment initiation with a high positive predictive value (~90%), independent of established clinical severity scores such as MELD and MDF. Notably, its predictive performance was preserved in patients with active infection and ACLF—

clinical contexts in which corticosteroid use is often controversial. Together, these findings indicate that SULT2A1-based stratification may complement existing clinical tools by identifying patients most likely to benefit from corticosteroid therapy, particularly in settings where liver biopsy is already performed due to diagnostic uncertainty or relative contraindications to treatment.

While the need for liver biopsy limits universal applicability, transjugular biopsy is frequently performed in suspected sAH, making this approach feasible in real-world settings. Future studies exploring non-invasive surrogates of mature hepatocyte identity, such as circulating transcriptomic or proteomic markers, may further broaden clinical implementation.

Beyond baseline prediction, longitudinal analyses revealed divergent parenchymal trajectories following corticosteroid therapy. By day 8, responders demonstrated enhanced hepatocyte regenerative activity, evidenced by an increased proportion of cycling hepatocytes, activation of hepatocyte growth factor–related signaling pathways, and higher Ki67 expression. In contrast, non-responders retained transcriptional signatures associated with cellular senescence, consistent with impaired regenerative capacity. These findings align with prior studies linking regenerative markers to survival in sAH and acute liver failure and reinforce the concept that recovery depends not only on dampening inflammation but also on restoring parenchymal function[28,32,33]. Our functional experiments further support an association between mature hepatocyte status and proliferative capacity. CRISPR–Cas9–mediated disruption of *SULT2A1* in hepatocyte-derived cells resulted in reduced cell growth and suppressed proliferative marker expression in vitro.

This study has limitations. Our data clearly points towards SULT2A1 being a marker of hepatocyte identity and regenerative competence. However, it remains uncertain if SULT2A1 directly modulates corticosteroid signaling or predicts therapy response solely based on its relation to hepatocyte functional reserve. Future studies incorporating single-nucleus transcriptomic profiling of patients who are not candidates for corticosteroid therapy may help delineate treatment-independent disease mechanisms and clarify whether baseline mature hepatocyte identity markers, such as SULT2A1 expression, specifically identify patients with a higher likelihood of spontaneous recovery. Studies with a higher number of untreated patients could also help separating treatment effects from natural disease progression. In-vitro

experiments investigating changes in corticosteroid responsiveness after *SULT2A1*-KO could give mechanistic insight into the potential link between SULT2A1 and corticosteroid treatment. Secondly, sequential biopsies were obtained one week apart, which may limit assessment of longer-term cellular remodeling. However, this interval ensured comparable corticosteroid exposure across patients, thereby minimizing treatment-related bias. Furthermore, reliance on histological scoring may constrain applicability in settings where biopsy is not feasible. In addition, prospective and multicenter studies will be required to fully define the predictive performance of the SULT2A1 score. Lastly, while CRISPR–Cas9–mediated *SULT2A1* disruption was associated with reduced proliferative capacity in hepatocyte-derived cells, we acknowledge that we did not include a non-targeting sgRNA control. Although genome editing was performed using transient ribonucleoprotein delivery of Cas9-HiFi nuclease, which minimizes prolonged nuclease activity and reduces off-target risk compared to plasmid-based systems, we cannot fully exclude the possibility that guide-dependent off-target cleavage or CRISPR-associated DNA damage responses contributed to the observed phenotype. Therefore, these experiments should be interpreted as supportive biological evidence linking SULT2A1 loss to impaired hepatocyte growth capacity rather than definitive proof of a direct mechanistic role. Nonetheless, the integration of discovery, validation, and functional analyses across independent cohorts strengthens the robustness and translational relevance of our findings.

In conclusion, we present the first single-nucleus transcriptomic atlas of sAH liver tissue stratified by treatment response and incorporating sequential biopsies. Our findings indicate that response to corticosteroid therapy reflects the combined influence of an inflammatory myeloid compartment that is responsive to corticosteroids and a hepatocyte compartment that retains mature hepatocyte identity and regenerative capacity. By using SULT2A1 as a marker of mature hepatocytes, we propose a clinically applicable approach for baseline patient stratification. Together, these insights improve understanding of sAH pathophysiology and support more tailored therapeutic strategies that integrate immune modulation with preservation of liver parenchymal function.

Acknowledgements

We would like to thank Thomas Van Brussel and Rogier Schepers for their practical support and Gino Philips and Dora Bihary for their bio-informatic support. We would like to thank the hospital staff of the service of hepatology, interventional radiology and intensive care for caring

for our patients. Lastly, we would like to thank the patients for their willingness to participate in this study.

Data availability statement

Raw sequence data is deposited European Genome-phenome Archive (EGA) under EGAD50000002317. The Shiny application is hosted on the shinyapps.io server and is available at: (https://ccb-bioit.shinyapps.io/sn-ah-atlasbrowser/). The R-script is available at https://osf.io/n9w4k/overview?view_only=633820bd0d9a4d3681d2086e7c967b17. Publicly available data was utilized for CIBERSORTx deconvolution and is accessible at GEO under GSE143318, GSE270042 and GSE167308 [9,25,26].

Figures

Figure 1: snRNA-sequencing liver atlas for sAH

A: Schematic overview of the experimental workflow. B: Annotated Uniform Manifold Approximation and Projection (UMAP) plot of integrated dataset at baseline. C: Marker gene expression per cell type at baseline (Heatmap). D: Cell type proportion at baseline (Boxplot, unpaired T-test). $**p_{adj}<0.01$, $***p_{adj}<0.001$, $****p_{adj}<0.0001$.

Figure 2: Influx of monocytes in sAH-R versus sAH-NR

A: Annotated UMAP plot of myeloid cells at baseline. B: Marker gene expression per cell type at baseline (Heatmap). C: Beeswarm plot comparing sAH-R and sAH-NR at baseline (MiloR, $p_{adj}<0.05$ shown in colour). D: Beeswarm plot comparing sAH-R and sAH-NR at day 8 (MiloR, $p_{adj}<0.05$ shown in colour). E: Average GSVA score of GO:BP pathways in monocytes. Ag = antigen, neg = negative, pos = positive. F: Percentual area of S100A8 positivity (Boxplot, Unpaired t-test or Mann-Whitney test). G: Representative IHC images of S100A8 per disease. H: Overview of S100A8 staining in sAH-R and sAH-NR on COMET. $*p_{adj}<0.05$, $**p_{adj}<0.01$

Figure 3: Loss of mature hepatocyte identity in sAH

A: Annotated UMAP plot of epithelial cells at baseline. B: Marker gene expression per hepatocyte subtype (Dotplot). C: Hepatocytes subtype proportion at baseline (Boxplot, Unpaired t-test). D: Overview of SULT2A1, YAP1, S100A8, AKR1B10, aSMA, CK18 in sAH-R and sAH-NR on COMET. E: Pseudotime analysis on epithelial subclusters (Monocle, 10.000 nuclei per subtype). F: Hepatocytes subtype proportion at baseline in sAH (Boxplot, Unpaired t-test). G: Volcano plot in hepatocytes, comparing sAH-R vs. sAH-NR (Wilcoxon Rank-Sum test). $\#p_{adj}<0.10$, $*p_{adj}<0.05$, $**p_{adj}<0.01$, $***p_{adj}<0.001$, $****p_{adj}<0.0001$.

Figure 4: Immunohistochemical validation of mature hepatocyte loss of identity

A: Percentual area of AKR1B10 positivity for healthy, AD and sAH (Boxplot, Mann Whitney test). B: Percentual area of AKR1B10 positivity in sAH-R and sAH-NR (Boxplot, Mann Whitney test). C: Representative IHC images of AKR1B10 per condition. D: Proportion of samples with SULT2A1 grade for healthy, AD and sAH (Barplot, Chi-squared test for trend). E: Representative IHC images of SULT2A1 per grade. F: Proportion of samples with SULT2A1 grade for sAH-R and sAH-NR (Barplot, Chi-squared test for trend). G: Overview of SULT2A1 staining in sAH-R and sAH-NR on COMET. *$p<0.05$, **$p<0.01$, ***$p<0.001$, ****$p<0.0001$

Figure 5: Development of SULT2A1 score

A: Correlation between *SULT2A1* expression and SULT2A1 staining in paired samples (Spearman correlation). B: Volcano plot comparing SULT2A1+ and SULT2A1- hepatocytes in sAH (Wilcoxon Rank-Sum test). C: Average GSVA score of GO:BP pathways in sAH hepatocytes. D: Proportion of samples with high SULT2A1 score in sAH-R vs sAH-NR (Chi-squared test). E: Proportion of samples with high SULT2A1 score in subset of patients with infection and ACLF grade 2-3 (Chi-squared test). F: 30-day mortality per SULT2A1 grade in sAH (Chi-squared for trend). G: Proportion of samples with SULT2A1 grade for non-corticosteroid treated sAH-R and sAH-NR (Barplot, Chi-squared test for trend). H: Correlation of SULT2A1-grade with baseline variables (Dotplot, Pearson correlation). *$p<0.05$, ***$p<0.001$, ****$p<0.0001$

Figure 6: Lack of hepatocyte regeneration in sAH-NR

A: Average GSVA score of GO:BP pathways in sAH hepatocytes. B: Cell type proportion of hepatocytes in paired samples (Boxplot, Unpaired t-test). C: Differential gene expression for cycling genes comparing sAH-R and sAH-NR at day 1 and 8, and SULT2A1 positive and SULT2A1 negative hepatocytes (Wilcoxon Rank-Sum test). D: Number of Ki67+ hepatocytes per high power field (Boxplot, Mann-Whitney test) E: Representative IHC images of Ki67 staining. *$p<0.05$, **$p<0.01$, ****$p<0.0001$

References

1. Bataller R, Arab JP, Shah VH. Alcohol-Associated Hepatitis. *N Engl J Med*. 2022;387(26):2436-2448. doi:10.1056/NEJMRA2207599
2. Thursz M, Gual A, Lackner C, et al. EASL Clinical Practice Guidelines: Management of alcohol-related liver disease. *J Hepatol*. 2018;69(1):154-181. doi:10.1016/j.jhep.2018.03.018
3. **Van Melkebeke L, Broekhoven AGC, Ostyn T**, et al. Patients with a History of Bariatric Surgery Are 8 Years Younger at Presentation with Severe Alcoholic Hepatitis. *Obes Surg*. 2023;33(1):284-292. doi:10.1007/S11695-022-06386-1
4. Van Melkebeke L, Korf H, Tsochatzis E, van der Merwe S, Nevens F, Verbeek J. Treatment of severe alcoholic hepatitis: A systematic review. *Curr Opin Pharmacol*. 2021;60:91-101. doi:10.1016/J.COPH.2021.06.011
5. Louvet A, Thursz MR, Kim DJ, et al. Corticosteroids Reduce Risk of Death Within 28 Days for Patients With Severe Alcoholic Hepatitis, Compared With Pentoxifylline or Placebo—a Meta-analysis of Individual Data From Controlled Trials. *Gastroenterology*. 2018;155(2):458-468.e8. doi:10.1053/j.gastro.2018.05.011

6. Mathurin P, O'Grady J, Carithers RL, et al. Corticosteroids improve short-term survival in patients with severe alcoholic hepatitis: Meta-analysis of individual patient data. *Gut*. 2011;60(2):255-260. doi:10.1136/gut.2010.224097
7. Thursz MR, Richardson P, Allison M, et al. Prednisolone or Pentoxifylline for Alcoholic Hepatitis. *New England Journal of Medicine*. 2015;372(17):1619-1628. Accessed February 25, 2020. https://pubmed.ncbi.nlm.nih.gov/25901427/
8. Argemi J, Latasa MU, Atkinson SR, et al. Defective HNF4alpha-dependent gene expression as a driver of hepatocellular failure in alcoholic hepatitis. *Nat Commun*. 2019;10(1):3126. doi:10.1038/S41467-019-11004-3
9. Bou Saleh M, Louvet A, Ntandja-Wandji LC, et al. Loss of hepatocyte identity following aberrant YAP activation: A key mechanism in alcoholic hepatitis. *J Hepatol*. 2021;75(4):912-923. doi:10.1016/J.JHEP.2021.05.041
10. Kim A, Wu X, Allende DS, Nagy LE. Gene deconvolution reveals aberrant liver regeneration and immune cell infiltration in alcohol-associated hepatitis. *Hepatology*. 2021;74(2):987-1002. doi:10.1002/HEP.31759
11. Aguilar-Bravo B, Ariño S, Blaya D, et al. Hepatocyte dedifferentiation profiling in alcohol-related liver disease identifies CXCR4 as a driver of cell reprogramming. *J Hepatol*. 2023;79(3):728-740. doi:10.1016/J.JHEP.2023.04.013
12. **Guilliams M, Bonnardel J, Haest B**, et al. Spatial proteogenomics reveals distinct and evolutionarily conserved hepatic macrophage niches. *Cell*. 2022;185(2):379-396.e38. doi:10.1016/J.CELL.2021.12.018
13. **Andrews TS, Nakib D**, Perciani CT, et al. Single-cell and spatial transcriptomics characterisation of the immunological landscape in the healthy and PSC human liver. *J Hepatol*. 2024;80(5):730-743. doi:10.1016/J.JHEP.2023.12.023
14. Ramachandran P, Dobie R, Wilson-Kanamori JR, et al. Resolving the fibrotic niche of human liver cirrhosis at single-cell level. *Nature*. 2019;575(7783):512-518. doi:10.1038/s41586-019-1631-3
15. **Van Melkebeke L, Verbeek J**, Bihary D, et al. Comparison of the single-cell and single-nucleus hepatic myeloid landscape within decompensated cirrhosis patients. *Front Immunol*. 2024;15:1346520. doi:10.3389/FIMMU.2024.1346520
16. **Gong T, Wang Y, Dong S**, et al. Single-cell RNA-seq reveals the communications between extracellular matrix-related components and Schwann cells contributing to the earlobe keloid formation. *Front Med (Lausanne)*. 2022;9:1000324. doi:10.3389/FMED.2022.1000324
17. **Estupiñán-Moreno E, Ortiz-Fernández L**, Li T, et al. Methylome and transcriptome profiling of giant cell arteritis monocytes reveals novel pathways involved in disease pathogenesis and molecular response to glucocorticoids. *Ann Rheum Dis*. 2022;81(9):1290-1300. doi:10.1136/annrheumdis-2022-222156
18. **Guan Y, Kim Y**, Wang Y, et al. Adipocyte death promotes hepatic infiltration of S100A8+ macrophages and steatotic liver disease progression in mice. *J Clin Invest*. 2025;135(21). doi:10.1172/JCI190635
19. **Cui A, Li B**, Wallace MS, et al. Single-cell atlas of the liver myeloid compartment before and after cure of chronic viral hepatitis. *J Hepatol*. 2024;80(2):251-267. doi:10.1016/j.jhep.2023.02.040
20. **Brosch M, Kattler K**, Herrmann A, et al. Epigenomic map of human liver reveals principles of zonated morphogenic and metabolic control. *Nat Commun*. 2018;9(1):4150. doi:10.1038/S41467-018-06611-5
21. Chi HC, Chen SL, Tsai CY, et al. Thyroid hormone suppresses hepatocarcinogenesis via DAPK2 and SQSTM1-dependent selective autophagy. *Autophagy*. 2016;12(12):2271-2285. doi:10.1080/15548627.2016.1230583

22. Govaere O, Cockell S, Tiniakos D, et al. Transcriptomic profiling across the nonalcoholic fatty liver disease spectrum reveals gene signatures for steatohepatitis and fibrosis. *Sci Transl Med*. 2020;12(572). doi:10.1126/SCITRANSLMED.ABA4448
23. **Andrews TS, Atif J**, Liu JC, et al. Single-Cell, Single-Nucleus, and Spatial RNA Sequencing of the Human Liver Identifies Cholangiocyte and Mesenchymal Heterogeneity. *Hepatol Commun*. 2021;6(4):821-840. doi:10.1002/HEP4.1854
24. Roskams T. Different types of liver progenitor cells and their niches. *J Hepatol*. 2006;45(1):1-4. doi:10.1016/j.jhep.2006.05.002
25. Guan Y, Peiffer B, Feng D, et al. IL-8+ neutrophils drive inexorable inflammation in severe alcohol-associated hepatitis. *J Clin Invest*. 2024;134(9). doi:10.1172/JCI178616
26. **Rodrigo-Torres D, Kilpatrick AM**, Ferreira-Gonzalez S, et al. Longitudinal paired liver biopsies and transcriptome profiling in alcohol-associated hepatitis reveal dynamic changes in cellular senescence. *Gut*. 2025;74(9):1500-1513. doi:10.1136/GUTJNL-2024-334094
27. Avila M, Dufour J, Gerbes A, et al. Recent advances in alcohol-related liver disease (ALD): summary of a Gut round table meeting. *Gut*. 2020;69(4):764-780. doi:10.1136/GUTJNL-2019-319720
28. Michalopoulos GK, Bhushan B. Liver regeneration: biological and pathological mechanisms and implications. *Nature Reviews Gastroenterology & Hepatology 2020 18:1*. 2020;18(1):40-55. doi:10.1038/s41575-020-0342-4
29. **Peng H, Feng K, Jia W**, Li Y, Lv Q, Zhang Y. An integrated investigation of sulfotransferases (SULTs) in hepatocellular carcinoma and identification of the role of SULT2A1 on stemness. *Apoptosis*. 2024;29(5-6):898-919. doi:10.1007/S10495-024-01938-5
30. Hardesty J, Hawthorne M, Day L, et al. Steroid responsiveness in alcohol-associated hepatitis is linked to glucocorticoid metabolism, mitochondrial repair, and heat shock proteins. *Hepatol Commun*. 2024;8(3). doi:10.1097/HC9.0000000000000393
31. He T, Tao B, Yi C, et al. 27-Hydroxycholesterol promotes metastasis by SULT2A1-dependent alteration in hepatocellular carcinoma. *Cancer Sci*. 2022;113(8):2575-2589. doi:10.1111/CAS.15435
32. Tornai D, Mitchell M, McClain CJ, et al. A novel score of IL-13 and age predicts 90-day mortality in severe alcohol-associated hepatitis: A multicenter plasma biomarker analysis. *Hepatol Commun*. 2023;7(12):e0296. doi:10.1097/HC9.0000000000000296
33. Rubio-Tomás T, Martí-Aguado D, Blaya D, et al. GDF15 is associated with hepatocellular senescence and correlates with mortality in patients with alcohol-associated hepatitis. *JHEP Reports*. 2025;7(9):101478. doi:10.1016/j.jhepr.2025.101478

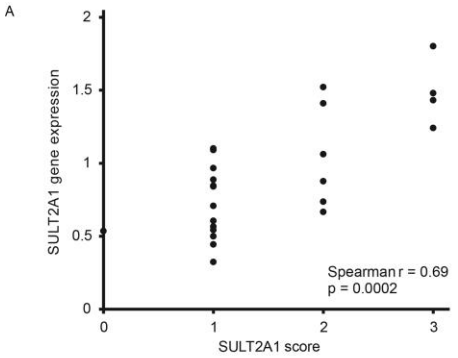

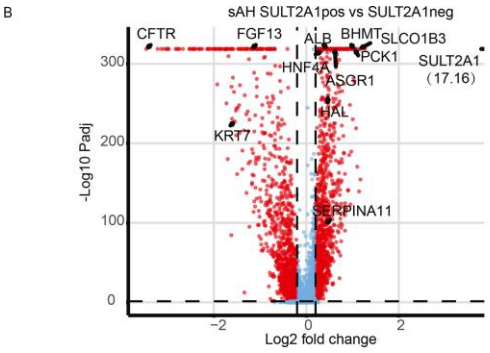

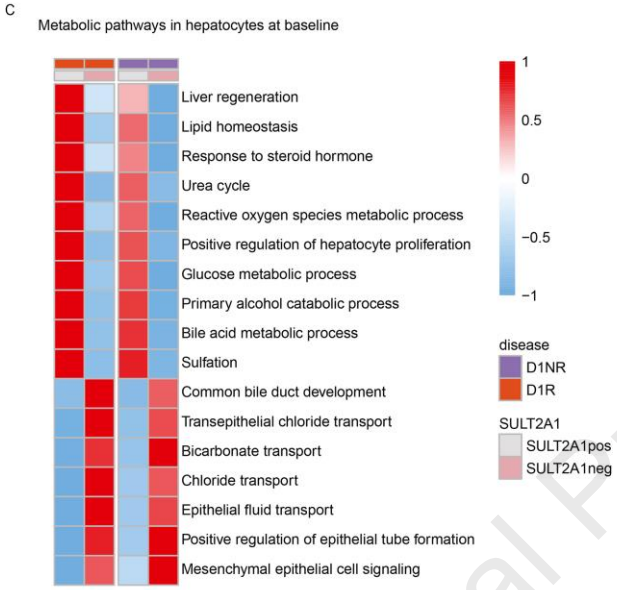

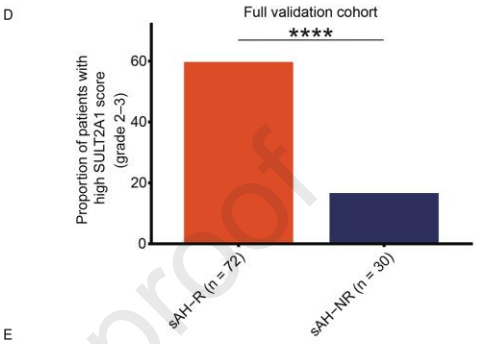

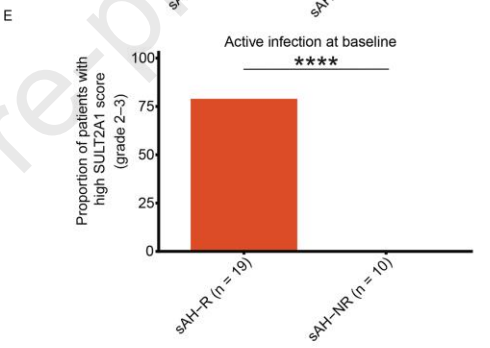

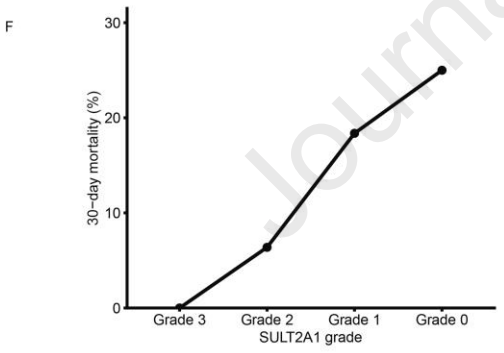

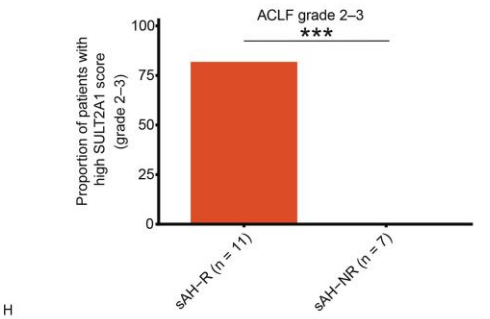

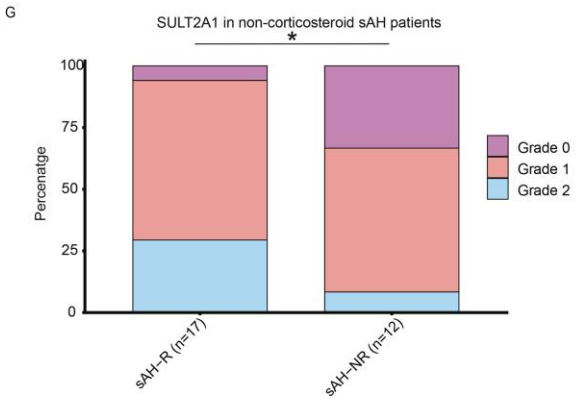

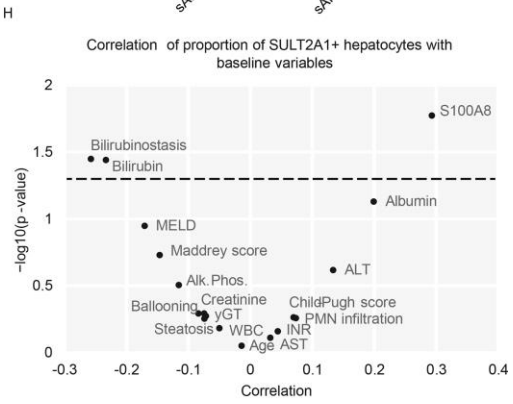

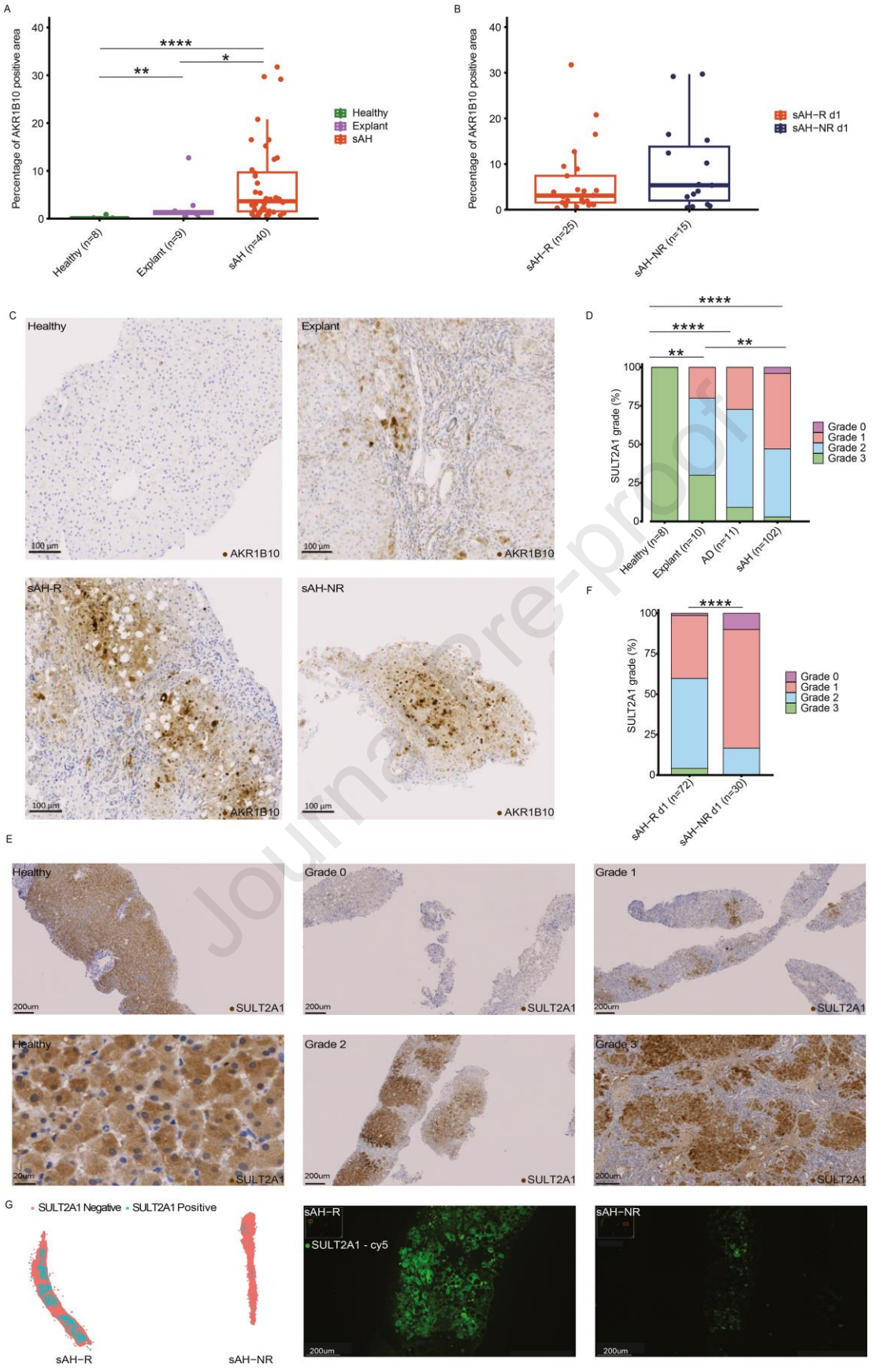

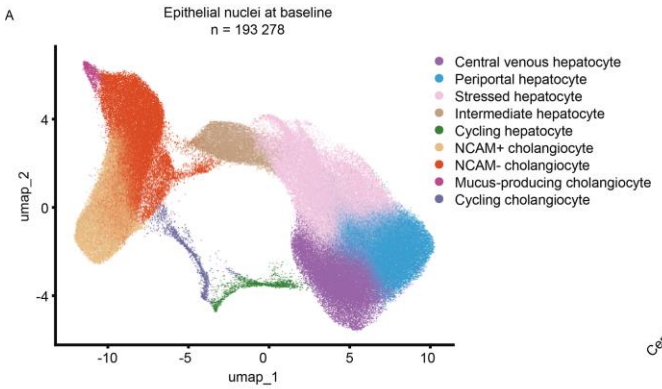

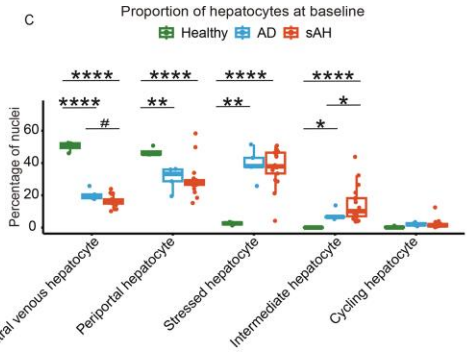

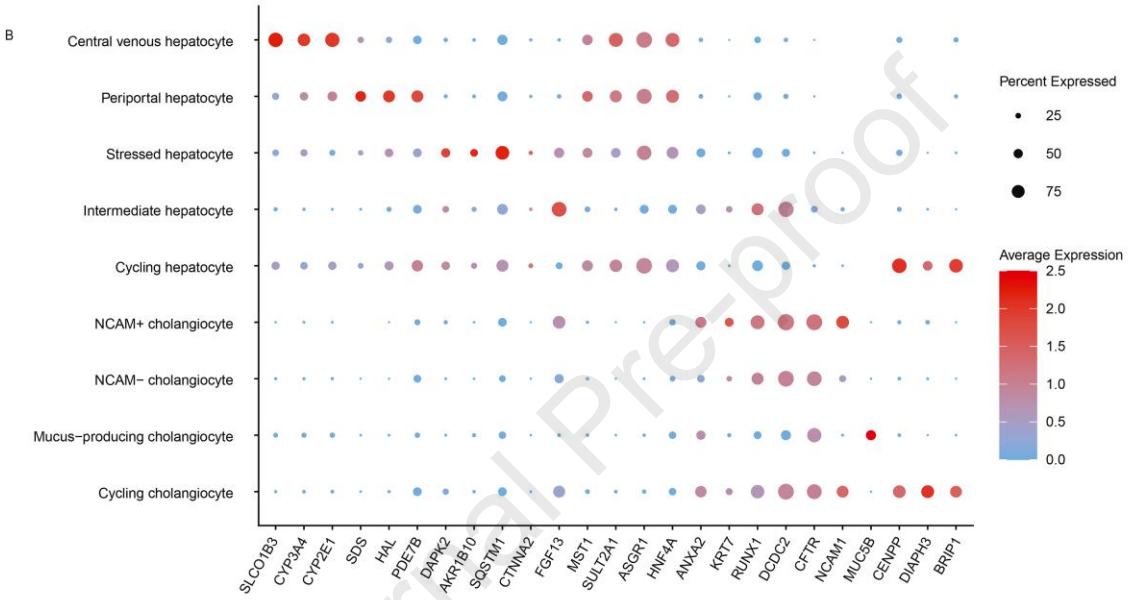

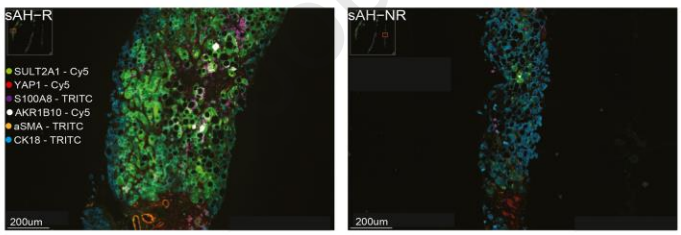

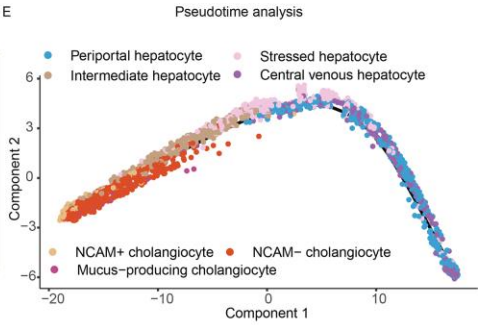

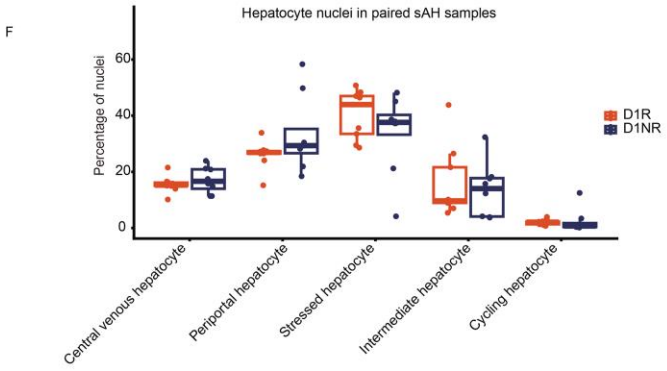

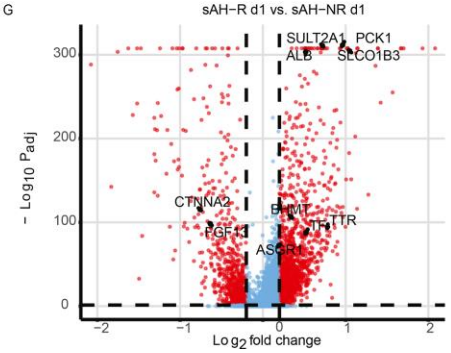

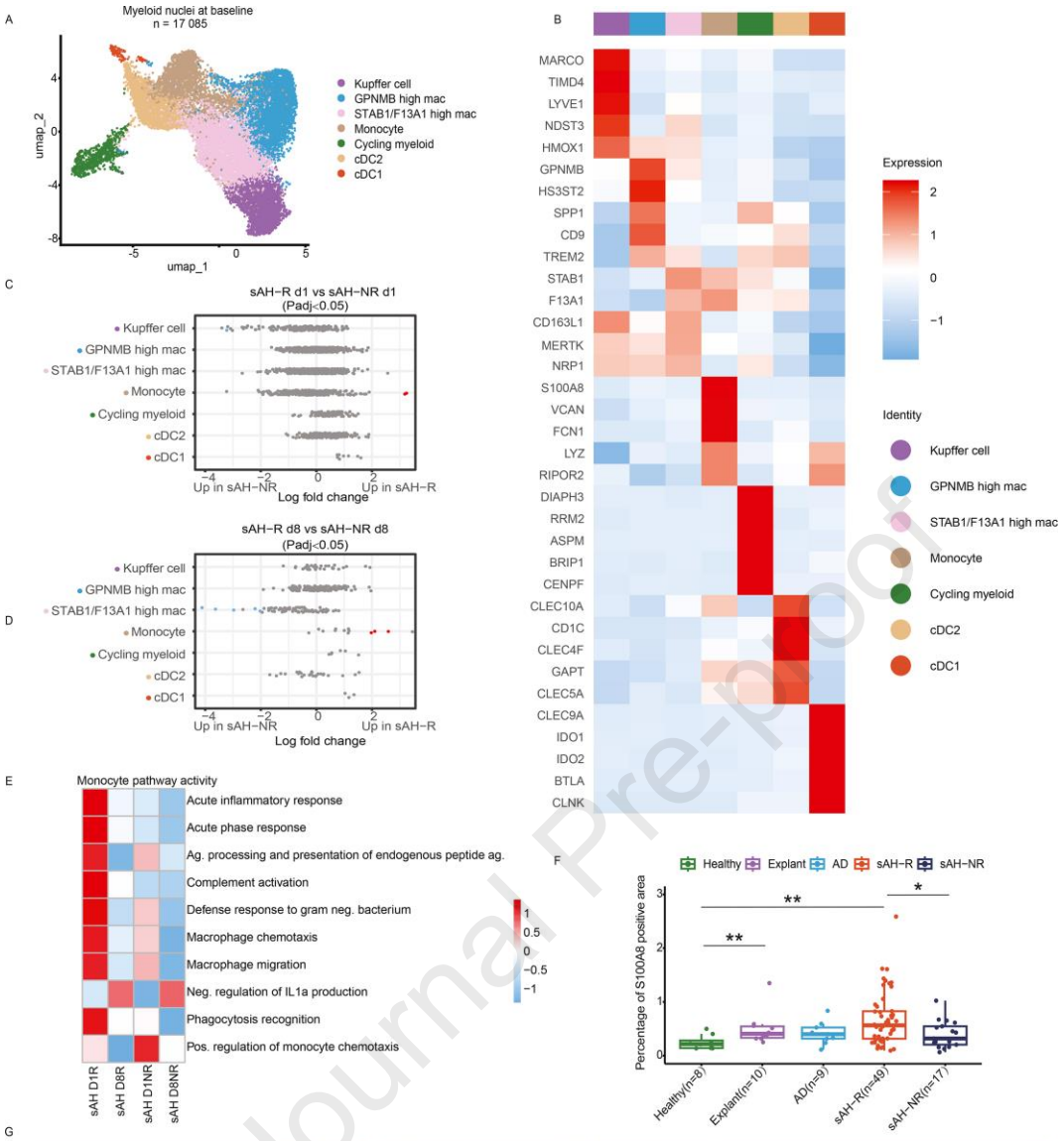
A
Myeloid nuclei at baseline
n = 17 085
umap_2
umap_1
Kupffer cell
GPNMB high mac
STAB1/F13A1 high mac
Monocyte
Cycling myeloid
cDC2
cDC1
B
MARCO
TIMD4
LYVE1
NDST3
HMOX1
GPNMB
HS3ST2
SPP1
CD9
TREM2
STAB1
F13A1
CD163L1
MERTK
NRP1
S100A8
VCAN
FCN1
LYZ
RIPOR2
DIAPH3
RRM2
ASPM
BRIP1
CENPF
CLEC10A
CD1C
CLEC4F
GAPT
CLEC5A
CLEC9A
IDO1
IDO2
BTLA
CLNK
Expression
Identity
C
sAH−R d1 vs sAH−NR d1
(Padj<0.05)
Up in sAH−NR
Up in sAH−R
Log fold change
D
sAH−R d8 vs sAH−NR d8
(Padj<0.05)
E
Monocyte pathway activity
Acute inflammatory response
Acute phase response
Ag. processing and presentation of endogenous peptide ag.
Complement activation
Defense response to gram neg. bacterium
Macrophage chemotaxis
Macrophage migration
Neg. regulation of IL1a production
Phagocytosis recognition
Pos. regulation of monocyte chemotaxis
sAH D1R
sAH D8R
sAH D1NR
sAH D8NR
F
Healthy
Explant
AD
sAH−R
sAH−NR
Percentage of S100A8 positive area
Healthy(n=8)
Explant(n=10)
AD(n=9)
sAH−R(n=49)
sAH−NR(n=17)

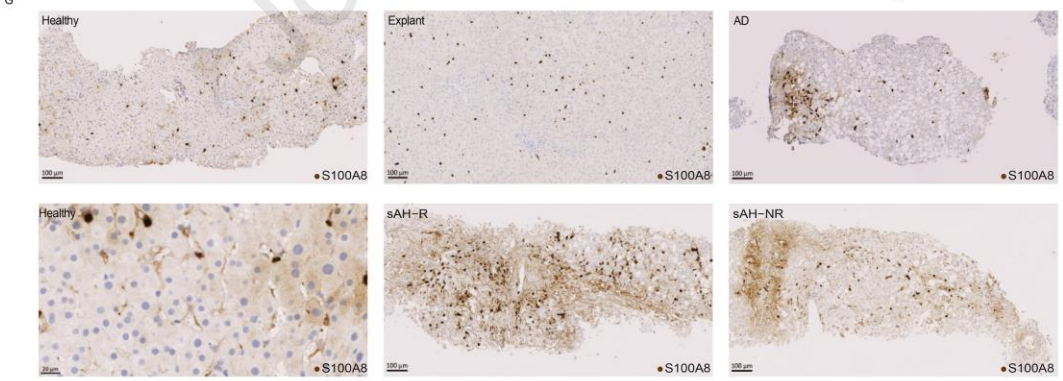
G
Healthy
Explant
AD
sAH−R
sAH−NR
S100A8

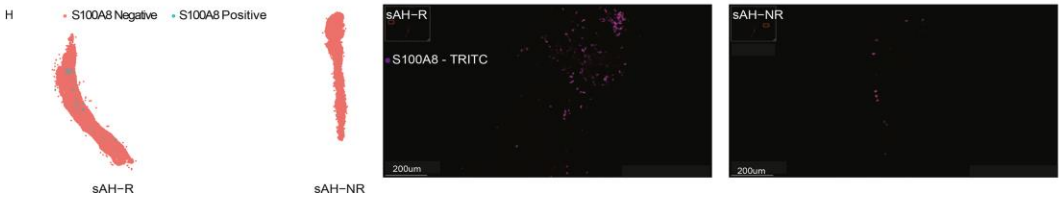
H
S100A8 Negative
S100A8 Positive
sAH−R
sAH−NR
S100A8 - TRITC
200um